Environmental Science & Technology

pubs.acs.org/est

Article

Production of Formate via Oxidation of Glyoxal Promoted by Particulate Nitrate Photolysis

Ruifeng Zhang, Masao Gen,* Tzung-May Fu, and Chak K. Chan*

Cite This: *Environ. Sci. Technol.* 2021, 55, 5711−5720

Read Online

ACCESS | Metrics & More | Article Recommendations | Supporting Information

ABSTRACT: Particulate nitrate photolysis can produce oxidants (i.e., OH, NO_2, and NO_2^-/HNO_2) in aqueous droplets and may play a potential role in increased atmospheric oxidative capacity. Our earlier works have reported on the SO_2 oxidation promoted by nitrate photolysis to produce sulfate. Here, we used glyoxal as a model precursor to examine the role of particulate nitrate photolysis in the formation of secondary organic aerosol (SOA) from particle-phase oxidation of glyoxal by OH radicals. Particles containing sodium nitrate and glyoxal were irradiated at 300 nm. Interestingly, typical oxidation products of oxalic acid, glyoxylic acid, and higher-molecular-weight products reported in the literature were not found in the photooxidation process of glyoxal during nitrate photolysis in the particle phase. Instead, formic acid/formate production was found as the main oxidation product. At glyoxal concentration higher than 3 M, we found that the formic acid/formate production rate increases significantly with increasing glyoxal concentration. Such results suggest that oxidation of glyoxal at high concentrations by OH radicals produced from nitrate photolysis in aqueous particles may not contribute significantly to SOA formation since formic acid is a volatile species. Furthermore, recent predictions of formic acid/formate concentration from the most advanced chemical models are lower than ambient observations at both the ground level and high altitude. The present study reveals a new insight into the production of formic acid/formate as well as a sink of glyoxal in the atmosphere, which may partially narrow the gap between model predictions and field measurements in both species.

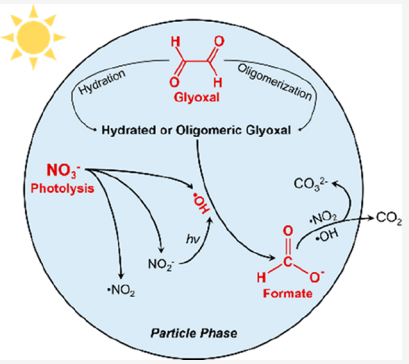

INTRODUCTION

Particulate nitrate is one of the major constituents of particulate matter (PM) and ubiquitously found in the atmosphere.[1,2] It has been reported to be photochemically reactive to form in-particle reactive species (e.g., OH, NO_2, and NO_2^-/HNO_2),[3−5] which are important oxidants and reactants in atmospheric particles. These oxidants will exert significant effects on the atmospheric oxidative capacity and promote the transformation of atmospheric species.[6−10] For instance, our recent works[6−8] demonstrated efficient SO_2 oxidation during nitrate photolysis, highlighting its important potential for enhancing the atmospheric oxidative capacity.

Organic aerosol, which can contribute 20−90% of atmospheric PM mass, can be emitted directly from combustion processes, such as biomass burning and fossil fuel combustion, or formed through a series of oxidation or aging processes of volatile organic compounds (VOCs).[11,12] However, the observed secondary organic aerosol (SOA) concentration and average oxidation state (oxygen-to-carbon ratio) usually are higher than those from model simulations.[13,14] The discrepancy between field measurements and model simulations could partly be ascribed to missing sources of in-particle oxidants or missing SOA formation mechanisms.[15,16] Huang et al.[17] found that aqueous SOA yields from photooxidation of both syringaldehyde and acetosyringone as model biomass burning compounds in bulk solutions containing nitrate are twice of those containing sulfate, likely due to the enhanced oxidizing capacity by nitrate photolysis. Together with our earlier work on prompt sulfate formation by in-particle nitrate photolysis,[6−8] such results suggest that particulate nitrate photolysis has potential to enhance in-particle oxidation processes and may hence contribute to the formation of SOA.

Glyoxal is one of the most abundant α-dicarbonyls in the atmosphere and has been extensively studied as an SOA precursor because it has a high effective Henry's law constant and can partition effectively into inorganic and organic aerosol.[18] It can be produced in high yields by the oxidation of anthropogenic and biogenic VOCs (e.g., toluene and isoprene)[19] and can be scavenged by cloud droplets/fogs due to its high water solubility. Glyoxal dissolved in cloud droplets/fogs undergoes a series of atmospheric processes[20,21] such as photochemical oxidation, acid/ammonium-catalyzed reactions, and oligomerization to form carboxylic acid, oligomers,

Received: December 4, 2020
Revised: March 31, 2021
Accepted: April 2, 2021
Published: April 16, 2021

https://doi.org/10.1021/acs.est.0c08199
Environ. Sci. Technol. 2021, 55, 5711−5720

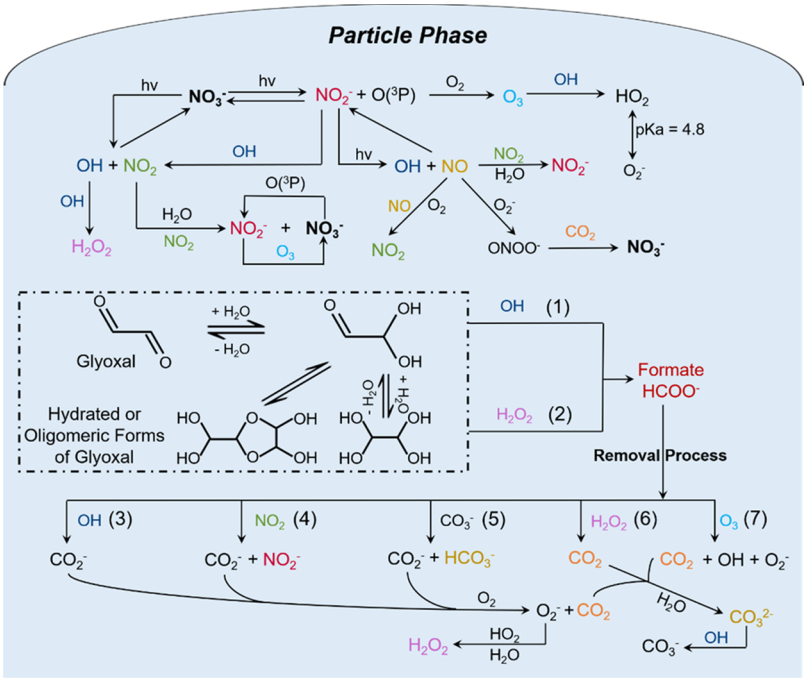

Figure 1. Reaction pathways in the oxidation of glyoxal during nitrate photolysis leading to the production of formate. The numbers 1 and 2 (in parentheses) indicate different formate production pathways, which are denoted as (1) [OH pathway]$_f$ and (2) [H_2O_2 pathway]$_f$ hereafter. The numbers 3−7 (in parentheses) indicate different formate removal pathways, which are denoted as (3) [OH pathway]$_r$, (4) [NO_2 pathway]$_r$, (5) [CO_3^- pathway]$_r$, (6) [H_2O_2 pathway]$_r$, and (7) [O_3 pathway]$_r$ hereafter. All reactions are summarized in Table S1. Note that glyoxal mainly exists as hydrated or oligomeric forms in particles.

organosulfate, and nitrogen-containing organics as SOA. The aqueous-phase oxidation of glyoxal by OH radicals is a well-known pathway to form SOA, in particular low-molecular-weight carboxylic acids (e.g., oxalic acid and glyoxylic acid) in cloud water where glyoxal is present at concentrations in the range of micro-molar (μM) concentrations.[20,22−25] On the other hand, during cloud droplet evaporation, glyoxal can be highly concentrated to reach up to M concentrations in aqueous tropospheric aerosol particles.[18,26] Previous studies have reported that high-concentration conditions facilitate the self-reactions to form oligomers that remain in the particle phase as SOA.[27,28] However, the fate of glyoxal and the oligomers in the aerosol phase under oxidation remains uncertain.

In this study, we investigate the oxidation of glyoxal to produce carboxylic acids during nitrate photolysis. We found that the OH radicals and H_2O_2 produced during nitrate photolysis can oxidize glyoxal into formic acid/formate. Note that formic acid/formate was found to be the main photoproduct in this study instead of the more commonly reported organic acids and higher-molecular-weight products (e.g., oxalic acid and tartaric acid),[20,22,23] as will be discussed in detail later. As shown in Figure 1, particulate nitrate can be photolyzed to produce first-generation oxidants (i.e., OH, NO_2, and NO_2^-/HNO_2), which may also undergo further radical reactions to form second-generation oxidants (e.g., H_2O_2).[29] Hydrated or oligomerized glyoxal can react with OH radicals as well as H_2O_2 to directly produce formic acid/formate.[23] Formic acid/formate is further oxidized into CO_2/CO_3^{2-}. In this paper, we will first discuss the dependence of the formate production rate on initial concentrations of nitrate and glyoxal. Then, a kinetic model, which builds on reported and proposed oxidation mechanisms, is used to elucidate the oxidation mechanisms.

MATERIALS AND METHODS

Materials. Aqueous stock solutions of sodium nitrate ($NaNO_3$; >99.0%, Acros Organics), sodium sulfate (Na_2SO_4; >99.0%, Acros Organics), sodium nitrite ($NaNO_2$; >97.0%, Acros Organics), sodium formate (formate; >99.0%, Acros Organics), and sodium carbonate (Na_2CO_3; >99.5%, VWR Chemicals BDH) were prepared by dissolving the corresponding salts into ultrapure water. Glyoxal (Gly; 40 wt % in water, Sigma-Aldrich) was diluted, and the diluted solution was mixed with the salt solution at a given mixing ratio. All chemicals were used without further purification. The premixed solution was atomized using a piezoelectric droplet generator (model 201, Uni-Photon, Inc.), and then, the resulting droplets were deposited on a hydrophobic substrate (model 5793, YSI, Inc.) with an optical transmission of >86% at 300 nm.[7] The droplets were equilibrated at 80% relative humidity (RH) for 60 min, and the equilibrated droplets were photolyzed using 300 nm UV irradiation (300 nm light-emitting diode lamp, M300L4, Thorlabs) subsequently. As shown in Figure S1a in the Supporting Information, the droplets achieved equilibrium with stable nitrate and Gly concentrations at around 30 min. The nominal particle size used for in situ Raman measurement was 55 ± 2 μm at equilibrium at 80% RH. Although we used particles that are larger than ambient fine particles, we analyzed the kinetic data using uptake coefficient of SO_2, which has taken size effects into consideration. The SO_2 uptake coefficient ($\sim 10^{-5}$) measured in our earlier works of SO_2 oxidation by particulate nitrate photolysis[6−8] falls in the magnitude order for the best match between model predictions and field measurements,[30] which has confirmed that results

https://doi.org/10.1021/acs.est.0c08199
Environ. Sci. Technol. 2021, 55, 5711−5720

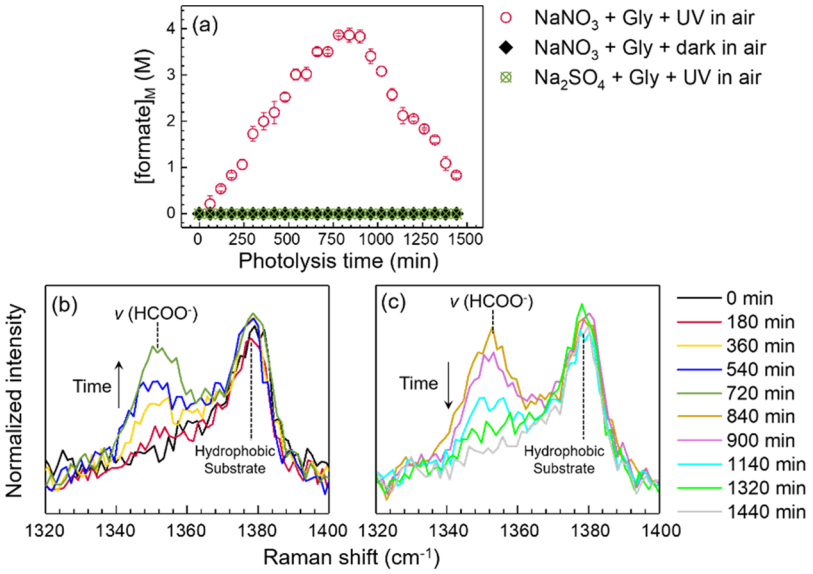

Figure 2. (a) Formate production under various conditions of premixed $NaNO_3$ + Gly in the presence or absence of 300 nm irradiation at $[NO_3^-]_0/[Gly]_0 = 1$ and of premixed Na_2SO_4 + Gly under 300 nm irradiation at $[SO_4^{2-}]_0/[Gly]_0 = 1$. (b,c) Time evolution of Raman spectra of formate during nitrate photolysis at $[NO_3^-]_0/[Gly]_0 = 1$. Subscript "0" denotes initial concentrations.

from these large droplets are applicable to ambient fine particles. The photon fluxes were quantified to be $\sim 1.7 \times 10^{15}$ photons cm^{-2} s^{-1} at 300 nm using a droplet containing a chemical actinometer of 2-nitrobenzaldehyde (2NB; >99.0%, Acros Organics) (Text S1).[31]

Photooxidation of Particles Containing Gly during Nitrate Photolysis and In Situ Raman Analysis. Photolysis of particles containing $NaNO_3$ + Gly at 300 nm was performed in a custom-made photochemical flow cell with two quartz windows for Raman analysis (top) and UV irradiation (bottom) (Figure S2). The RH in the flow cell was controlled using two gas streams of wet and dry air or nitrogen (N_2; >99.995%, <10 ppm O_2). Raman spectra were obtained at 100−4000 cm^{-1} using Raman spectroscopy (EnSpectr R532, EnSpectr) with a 20−30 mW 532 nm laser coupled with an optical microscope (CX41 Olympus). A 50× objective lens (numerical aperture of 0.35, SLMPLN50X, Olympus) was used to focus the laser onto the particle. The photooxidation products from the reacted particles were characterized using an ion chromatograph (IC) (ICS-1100, Dionex) with an IonPac AS15 analytical column, an AG15 guard column, and a conductivity detector. For IC analysis, five hydrophobic substrates with the particles containing $NaNO_3$ + Gly deposited were used, and each was sampled at different time intervals after reactions. The reacted particles on the substrate were dissolved in 1 mL of pure water, following IC analysis.

In this study, the main product from Gly oxidation was found to be formic acid/formate based on in situ Raman and IC measurement (Figure S3). Because the stable particle pH during reactions is around 6 (Figure S4), the product exists as formate ($HCOOH/HCOO^-$, pK_a = 3.8),[32] and hence, evaporation of formic acid is minor. Formate has the strongest Raman signal at ~1353 cm^{-1} (δ(C−H) mode, Figure S3a),[33] and this peak was used to calculate formate concentration. Gaussian fitting (Igor Pro, Wavemetrics) was used to calculate the Raman peak area of $\nu(NO_3^-)$, $\nu(HCOO^-)$, and $\nu(OH)_{water}$ at ~1047, ~1353, and ~3400 cm^{-1}, $A(NO_3^-)$, $A(HCOO^-)$, and $A(OH)_{water}$, respectively. In addition, the broadband ν(C−H) mode at 2900−3000 cm^{-1} normalized by $A(OH)_{water}$, $A(Gly)/A(OH)_{water}$, was used to represent the change in Gly concentration, [Gly], during reactions. It should be noted that formate may also contribute partially to the ν(C−H) intensity. However, its contributions to the ν(C−H) mode at 2900−3000 cm^{-1} can be neglected, as confirmed from Raman spectra of pure particulate sodium formate equilibrated at 80% RH (Figure S3a). In aqueous solutions, Gly mainly exists in the hydrated form (e.g., geminal diol) (Text S2).[34] Generally, hydrogen abstraction from the C−H moiety associated with the α position of the diol by OH radicals is energetically more favorable than that from the O−H moiety of the diol,[35,36] and hence, we used the ν(C−H) mode to monitor the changes of [Gly]. Formate concentration, [formate], was quantified based on the established calibration curve of [formate] of different standard sodium formate solutions versus the $A(HCOO^-)/A(OH)_{water}$ (Figure S5a).[7,8] The initial nitrate concentration, $[NO_3^-]_0$, was calculated based on the same method with the formate quantification (Figure S5b). The slight fluctuation in the Raman peak area ratio of $A(NO_3^-)/A(Gly)$ during the equilibrium process shown in Figure S1b suggested that water uptake/equilibrium or gas-aqueous equilibrium of Gly does not significantly affect the nominal mixing ratio. Hence, the initial Gly concentration, $[Gly]_0$, was estimated based on a given mixing ratio of $[NO_3^-]_0/[Gly]_0$. These initial concentrations (Table S2) were used as initial conditions in the kinetic modeling.

Kinetic Model Simulation. To better understand the mechanisms of Gly oxidation during nitrate photolysis, a kinetic model was constructed based on the reported and proposed mechanisms. Time-dependent [formate] estimated from the kinetic model was fitted to the experimentally measured [formate], $[formate]_M$, using the nitrate photolysis rate constant, j_{NO3-}, as a fitting parameter. j_{NO3-} may vary with particle composition and light intensity,[4,5] and hence, j_{NO3-} may differ among experiments. The fitting of j_{NO3-} has taken the uncertainties of UV irradiation into consideration. In addition to j_{NO3-}, the reaction rate constants of Gly + 2OH → $2HCOO^- + 2H^+$ and $NO_2 + HCOO^- \rightarrow NO_2^- + CO_2^- + H^+$

https://doi.org/10.1021/acs.est.0c08199
Environ. Sci. Technol. 2021, 55, 5711−5720

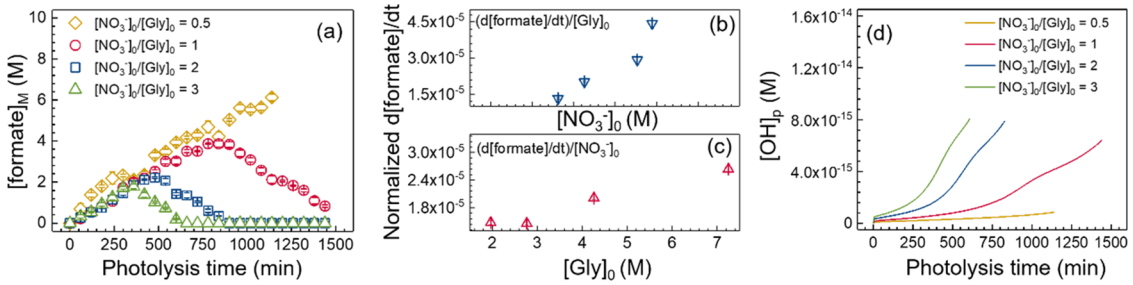

Figure 3. (a) $[\text{formate}]_M$ as a function of photolysis time during Gly oxidation promoted by nitrate photolysis at different $[NO_3^-]_0/[\text{Gly}]_0$ in air. Normalized initial formate production rate, (d $[\text{formate}]/\text{d}\,t)/[\text{Gly}]_0$ or (d $[\text{formate}]/\text{d}\,t)/[NO_3^-]_0$, as a function of (b) $[NO_3^-]_0$ and (c) $[\text{Gly}]_0$. (d) Model-predicted [OH] concentration, $[\text{OH}]_p$, as a function of time at different $[NO_3^-]_0/[\text{Gly}]_0$. Formate production rates are 96 ± 3, 86 ± 1, 81 ± 2, and 87 ± 2 $\mu M \cdot s^{-1}$ at $[NO_3^-]_0/[\text{Gly}]_0$ of 0.5, 1, 2, and 3, respectively.

in Figure 1 (R16[23] and R21[32] in Table S1, respectively) were adjusted in the kinetic model because the reaction rate constants are not well-documented in the literature. Carbonyl compounds have been reported to form gem diols, which are subsequently oxidized to form organic acids in the aqueous phase.[22,25,37] Hence, the aforementioned reaction mechanism of OH radicals with Gly was incorporated into our kinetic modeling. Hydrogen abstraction of $HCOO^-$ by NO_2 has recently been reported by Chen et al.[32] The decay process of formate can yield more CO_2^-, which has high reactivity with O_2 (2.4×10^9 M^{-1} s^{-1}, Table S1) to generate CO_2 and subsequently carbonate (CO_3^{2-}) (Figure 1). Nozière et al.[38] found that Gly can react efficiently in CO_3^{2-} solution. Hence, a consumption pathway of Gly by its reaction with CO_3^{2-} was proposed and incorporated in the current kinetic modeling (Text S3 and R18 in Table S1). These three rate constants of R16, R18, and R21 were also adjusted so that model predictions fit the $[\text{formate}]_M$, and the fitted rate constants are summarized in Table S1.

RESULTS AND DISCUSSIONS

Production of Formate by Gly Oxidation during Nitrate Photolysis. In the present study, glyoxylic and oxalic acids, which are typically identified as first- and second-generation products of Gly oxidation by OH radicals in dilute solutions,[22,23,25] respectively, were not observed (Figure S3). High-molecular-weight products (e.g., tartaric acid, malonic acid, and their oligomers), which were found at high Gly concentration in a previous study,[20] were also not detected by Raman spectroscopy and IC measurements (Figure S3). Interestingly, formate was found as the main photooxidation product from the concentrated Gly oxidation by particulate nitrate photolysis, which is also detected by the IC measurement (Figure S3). Figure 2a illustrates that the formate concentration under particulate nitrate photolysis in air (red circles) increases linearly with time and then decreases. The Raman spectra normalized by the $\nu(\text{OH})_{\text{water}}$ peak intensity clearly display an increasing trend of the formate peak intensity before 780 min and a decreasing trend afterward (Figure 2b,c). Furthermore, the nitrate concentration, $[NO_3^-]$, and $A(\text{Gly})/A(\text{OH})_{\text{water}}$ both show a clear decreasing trend during Gly oxidation (Figure S6). No formate peak (~1353 cm^{-1}) was observed in the absence of nitrate or UV irradiation (Figure S7), suggesting the participation of nitrate photolysis in the Gly oxidation in formate production. The effect of UV light intensity on the formate production rate is also ascertained. Figure S8 shows a higher formate production rate at higher light intensity. These results confirm the photooxidation of Gly to produce formate during nitrate photolysis.

The finding of formate as the major product of the reactions is different from the reaction products (e.g., oxalic acid, tartaric acid, and oligomers) reported in the literature.[20,22,23,25] The different observations between the present study and previous studies may suggest that reactions occurring in different environments (e.g., cloud droplets versus evaporating cloud droplets) do not necessarily proceed by the conventional mechanisms.[39] Typically, much lower glyoxal concentrations (i.e., a few mM or even lower) were used to mimic cloud/fog oxidation processes in previous studies.[22−25] In contrast, our experiments with droplets used much higher glyoxal concentration (i.e., a few M) to simulate oxidation processes in deliquesced aerosols. This concentration difference may lead to the different structural forms of glyoxal in the bulk phase (previous studies) and droplets (this study) for oxidation reactions. Specifically, the glyoxal monomer is the most abundant form in dilute aqueous glyoxal solution. In contrast, the glyoxal dimers or larger oligomers may dominate in the concentrated droplet.[28,39] Wilson et al.[40] suggested that microdroplets may enhance the overall importance of interfacial phenomena compared to the bulk phase, where reaction rates, mechanisms, and product distribution may be modified due to partial solvation and molecular alignment near surfaces. Earlier studies[20,25,37] have suggested that formic acid can be produced but as a second-generation product. For example, bulk aqueous reaction conducted by Lee et al.[25] suggested that glyoxylic acid produced from the Gly oxidation reacts with H_2O_2 to produce formic acid as a secondary product. They also proposed that the formation of larger organic acids (e.g., tartaric acid) or even oligomers via aqueous oxidation of glyoxal and subsequently their oxidation by OH radicals may further yield low-molecular-weight organic acids (e.g., glyoxylic acid and formic acid).[25] Zhao et al.[37] reported that the addition of H_2O_2 to the aldehyde group in Gly results in 2-hydroxy-2-hydroperoxyethanal (HHPE), which can be oxidized by OH radicals to produce formic acid. Lim et al.[20] suggested a minor pathway for formic acid production: Gly oxidation in the presence of O_2 (air) by OH radicals to produce peroxy radicals and their self-reactions to form an alkoxy, which then decomposes to formic acid. However, formate in this study is highly likely a first-generation product due to its prompt increase in concentration (Figure 2a). Formic acid may be directly produced from the Gly oxidation by OH radicals and H_2O_2.[22−24] Specifically, nucleophilic attack on the C−H group of hydrated or oligomeric Gly by OH radicals may directly produce formate when OH radicals can

https://doi.org/10.1021/acs.est.0c08199
Environ. Sci. Technol. 2021, 55, 5711−5720

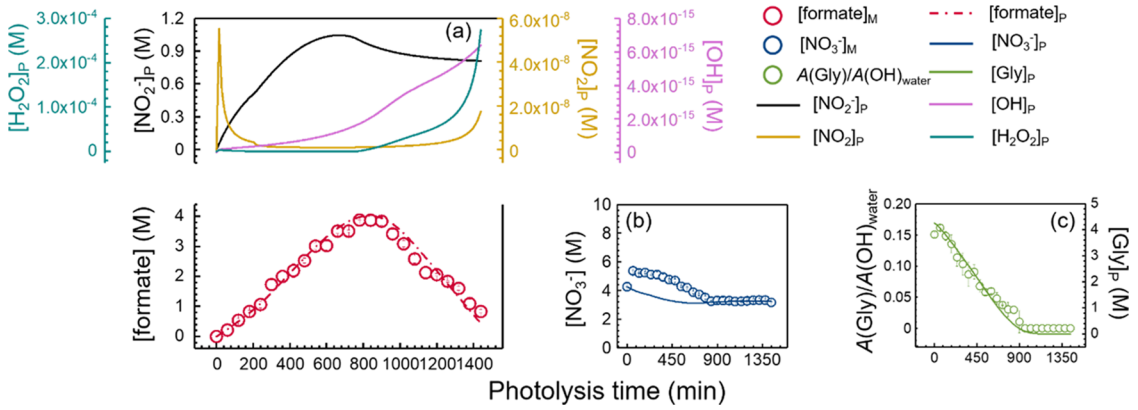

Figure 4. Oxidation of glyoxal by nitrate photolysis at $[NO_3^-]_0/[Gly]_0$ = 1 under 300 nm irradiation. The marker represents the data from experiments. Dash-dotted and solid lines represent the predicted time profiles of species concentration from kinetic modeling. The reproduced formate production at $[NO_3^-]_0/[Gly]_0$ = 0.5, 2, and 3 is shown in Figure S19. The fitted nitrate photolysis rate constants are $(1.5 \pm 0.05) \times 10^{-5}$ s^{-1} at different $[NO_3^-]_0/[Gly]_0$ in this study.

be produced efficiently from nitrate photolysis in the particle phase.[35] There is additional experimental evidence of the direct Gly oxidation by H_2O_2.[23,25] Thus, we incorporated these two Gly oxidation processes by OH and H_2O_2 for direct formate production in our kinetic modeling.

Effect of $[NO_3^-]_0/[Gly]_0$ on Formate Production. Figure 3a shows production and removal of formate at various $[NO_3^-]_0/[Gly]_0$. The highest formate concentration during reactions increases with $[Gly]_0$ (i.e., decreasing $[NO_3^-]_0/[Gly]_0$) (Figure 3a). Formate concentration normalized by $[Gly]_0$ shows a comparable maximum at various $[NO_3^-]_0/[Gly]_0$ (Figure S9a). At $[NO_3^-]_0/[Gly]_0$ = 0.5, formate removal was not observed, likely because there was still available Gly at the end of the experiment (Figure 3a and Figure S6e). From the trend of the datasets at higher ratios, it can be extrapolated that formate would decrease after some time eventually due to the complete consumption of Gly and further oxidation of formate. The initial formate production rate is found to be not sensitive to $[NO_3^-]_0/[Gly]_0$ (Figure 3a). Increasing $[NO_3^-]_0$ to increase the ratio leads to the corresponding decrease in $[Gly]_0$ in the particle phase at a given RH (Table S2), and these two combined effects may counteract each other to yield similar formation rates (Figure 3a) at different $[NO_3^-]_0/[Gly]_0$ ratios. The initial formate production rates were normalized by $[Gly]_0$ and $[NO_3^-]_0$ to investigate the individual effect of $[NO_3^-]_0$ and $[Gly]_0$ on formate production, respectively (Figure 3b,c). The normalized formate production rate increases as $[NO_3^-]_0$ increases (Figure 3b and Figure S9a), which is attributable to increased production rates of oxidants from nitrate photolysis. As shown in Figure 3d, the kinetic model predicts that the formation rate of OH radicals increases with $[NO_3^-]_0/[Gly]_0$ since Gly oxidation by OH radicals formed from nitrate photolysis is the dominant formate production pathway in this study, as will be discussed in detail later. Figure S10b also shows a good linear relation between the formate production rate and $[NO_3^-]_0$ when $[Gly]_0$ was fixed in the kinetic modeling. In combination with experimental results (Figure 3b), it indicates that formate production linearly increases with increasing $[NO_3^-]_0$. On the other hand, the effect of $[Gly]_0$ is not significant in the formate production rates at $[Gly]_0$ < 3 M, but the formation rate increases as $[Gly]_0$ increases further (Figure 3c and Figure S9b). The significant formate production at the aerosol-relevant concentration of Gly implies that aerosol-phase oxidation of Gly by OH radicals may not significantly contribute to SOA formation because formic acid is a volatile component.

Kinetic Simulation of Gly and Formate Oxidation Processes during Nitrate Photolysis. Figure 4 shows that the predicted formate concentration ($[formate]_P$) monotonically increases to its maximum at a photolysis time of 780 min and then decreases afterward, which agrees well with the measured formate concentration ($[formate]_M$). $[formate]_P$ decreases after predicted Gly concentration ($[Gly]_P$) is consumed completely, which is also consistent with the observed decay of $A(Gly)/A(OH)_{water}$ based on in situ Raman measurement (Figure 4c and Figure S6). Measured nitrate concentrations ($[NO_3^-]_M$) and $A(Gly)/A(OH)_{water}$ both show a slight increase from 0 to 60 min (Figure 4b,c and Figure S6). As shown in Figure S11, a slight decrease in particle size was observed initially, suggesting that there was less water in the particles, and hence, nitrate concentration increased initially during its photolysis. We also attribute the shrinkage of particle size to the partial evaporation of products (NO_2^-/HONO, pK_a = 3.2; $HCOO^-$/HCOOH, pK_a = 3.8), resulting from the low initial pH (Figure S4). It should be noted that the initially increased nitrate and Gly concentrations are more pronounced at low $[NO_3^-]_0/[Gly]_0$ (Figure S6). Figure S4 shows that there is a higher initial pH at high $[NO_3^-]_0/[Gly]_0$, and subsequently, they reached up to similarly stable pH (~6) among different conditions. No noticeable change in particle size was observed at the later stage further (Figure S11). Thus, the particle size during the overall course of photolysis should not affect the photochemistry significantly. The reduced water content due to partial evaporation of products was not simulated in our kinetic modeling, and hence, there may be some discrepancy between the measured and the predicted concentrations.

As mentioned earlier, two Gly oxidation mechanisms by H_2O_2 and OH radicals for direct formate production were incorporated in our current model as reactions of Gly + H_2O_2 → $2HCOO^-$ + $2H^+$ ($[H_2O_2$ pathway$]_f$ in Figure 1) and Gly + 2OH → $2HCOO^-$ + $2H^+$ ($[OH$ pathway$]_f$ in Figure 1), respectively. The $[formate]_P$ is found not to be sensitive to the rate constant of $[H_2O_2$ pathway$]_f$ in this study (Figure S12). Hence, the previously reported rate constant of ~1 M^{-1} s^{-1} was used in the model without adjustment.[23] The rate constant of the $[OH$ pathway$]_f$ was adjusted to fit $[formate]_M$. The [OH

https://doi.org/10.1021/acs.est.0c08199
Environ. Sci. Technol. 2021, 55, 5711−5720

pathway]$_f$ for formate production is not a well-known process compared to the [H_2O_2 pathway]$_f$. Therefore, nitrite photolysis was used as a source of OH radicals to further investigate the [OH pathway]$_f$.[41] The experiments were performed using photolysis of droplets containing $NaNO_2$ + Gly in air. As shown in Figure S13a,b, a rapid increase in formate production was observed, and the Raman peak intensity of Gly and nitrite clearly decreased. To examine the potential role of direct oxidation of Gly by nitrite, dark experiments were also performed with premixed droplets of $NaNO_2$ + Gly in air (Figure S13c), while the other conditions were the same as before. The formate production rate under the dark condition is too low to explain the rapid formate production found under photolysis (Figure S13a). We further conducted an experiment with particles containing $NaNO_3$ + Gly under 254 nm irradiation (Model 33SC-9, Pen-Ray, Analytik Jena, US), where the main photoproducts are OH radicals and NO_2 from nitrate photolysis[29] to ascertain the role of OH radicals in Gly oxidation. The results clearly show a rapidly emerging formate peak (Figure S14), which further supports our hypothesis of the role of OH radicals. Note that NO produced from nitrite photolysis and NO_2 generated by nitrate photolysis both are suggested to be reactive toward Gly in the gas phase, but such reactions do not yield formic acid,[42−44] and their aqueous-phase reactions have not been reported. Consequently, such reactions were not relevant in this study. Together with earlier experiments of Gly oxidation by nitrite photolysis, these results strongly suggest that direct formate production from the Gly oxidation by OH radicals is feasible. Moreover, the kinetic modeling illustrates that the [OH pathway]$_f$ is the main contributor to formate production (~96%) based on the sensitivity test of the [OH pathway]$_f$ and [H_2O_2 pathway]$_f$ on formate production at $[NO_3^-]_0/[Gly]_0$ = 1 (Figure S15). The fitted rate constant of Gly + 2OH → $2HCOO^-$ + $2H^+$ in this study is 4.5×10^{10} M^{-1} s^{-1}, which is consistent with that of other investigators who note that aqueous-phase reaction of OH radicals with organics containing C−H or C−C multiple bonds generally occurs at or near diffusion limits (i.e., ~10^{10} M^{-1} s^{-1}).[36] Note that such a fitted rate constant is seven orders of magnitude higher than that reported by Carlton and coauthors, although they observed rapidly emerging formate peaking within 2−3 min and disappeared almost completely in 30 min in their bulk experiments.[23] There is growing evidence that chemical reactions can be accelerated by many orders of magnitude (10 to 10^6) relative to the bulk phase when such reactions are confined in microdroplets, thin films, and emulsions.[40,45] Consequently, accelerated reaction rates would be reflected by fitted rate constants in the kinetic modeling. As shown in Figure 4a, the predicted concentration of OH radicals ($[OH]_P$) continuously increases as the reaction proceeds, which implies that the consumption rate of OH radicals decreases due to the reduced [Gly]. The $[OH]_P$ remains low when Gly is available, and it increases faster after Gly is consumed completely, suggesting that Gly is the main species consuming OH radicals. In addition, the predicted NO_2 concentration ($[NO_2]_P$) increases initially and then rapidly decreases, which is attributed to its consumption by formate. Since NO_2^- is not involved in Gly oxidation directly, its concentration ($[NO_2^-]_P$) remains high and increases due to continuous nitrate photolysis before 780 min. In addition to nitrate photolysis, the reaction of NO_2 with formate can also yield NO_2^- production ([NO_2 pathway]$_r$ in Figure 1) since the [NO_2 pathway]$_r$ is one of the main removal pathways of formate, as will be discussed next.

The decrease in formate concentrations after Gly depletion (Figure 4a) is likely driven by the oxidation of formate by oxidants produced from nitrate photolysis (Figure 1). Experiments with premixed $NaNO_3$ + formate at different initial molar ratios of NO_3^- to formate, $[NO_3^-]_0/[formate]_0$, under irradiation or dark conditions were performed to verify it. As shown in Figure S16, an obvious decrease in formate concentration is observed during nitrate photolysis, whereas there is no significant decrease of formate under dark conditions, confirming that formate is oxidized by the photoproducts from nitrate photolysis. Although CO_3^- and O_3 can react with formate ([CO_3^- pathway]$_r$ and [O_3 pathway]$_r$ in Figure 1), they are third-/fourth-generation oxidants, and hence, their contribution to formate removal is likely to be minor. Kinetic modeling results confirm that the [CO_3^- pathway]$_r$ and [O_3 pathway]$_r$ only contributed to <5% of formate removal in total (Figure S17b, d, and f). Accordingly, the role of first-/second-generation oxidants on the decay of formate was investigated. We examined the contributions of the [NO_2 pathway]$_r$, [OH pathway]$_r$, and [H_2O_2 pathway]$_r$ to the removal process of formate in the kinetic modeling. Simulation results show that the [NO_2 pathway]$_r$ (~50%) contributes to most of the formate removal followed by the [H_2O_2 pathway]$_r$ and [OH pathway]$_r$ (Figure S17b, d, and f). This is also reflected by the only small increase in $[NO_2]_P$ and a faster increasing $[OH]_P$ and H_2O_2 concentration ($[H_2O_2]_P$) after 780 min (Figure 4a). The fitted rate constant of NO_2 + $HCOO^-$ → NO_2^- + CO_2^- + H^+ is 1.0×10^4 M^{-1} s^{-1} in this study, which is one order magnitude smaller than that reported by Chen et al. (5.0×10^5 M^{-1} s^{-1}).[32]

As shown in Figure 4b, no obvious decrease in the $[NO_3^-]_M$ at $[NO_3^-]_0/[Gly]_0$ = 1 was observed during the formate removal process, which is consistent with the trend of $[NO_3^-]_M$ in the experiments with irradiated premixed particles of $NaNO_3$ + formate (Figure S17a, c, and e). The same observations were also made at $[NO_3^-]_0/[Gly]_0$ = 2 and 3 as well as from kinetic model results (Figure 4b and Figure S6c,d). After formate was consumed completely, a further decrease in nitrate concentration was observed (Figures S6c,d and S18a), likely due to further nitrate photolysis. Hence, reaction products produced during the formate removal process may be involved in regenerating nitrate. We speculated the reaction of NO and O_2^- to form $ONOO^-$, which can react with CO_2 to yield NO_3^-.[32,46] The reactions replenish NO_3^- loss in photolysis. This process requires O_2, and hence, premixed particulate $NaNO_3$ + formate reaction at different $[NO_3^-]_0/[formate]_0$ was conducted in a N_2 environment to verify our hypothesis. As shown in Figure S18, a clear decrease in nitrate concentration was observed in N_2. The difference of $[NO_3^-]_M$ decay percentage between air and N_2 becomes smaller as $[NO_3^-]_0/[formate]_0$ increases, which confirms that products produced from the formate removal process play a crucial role in regenerating nitrate (Figure S18). Kinetic modeling results without the speculated NO_3^- regeneration mechanism also show a reduction of NO_3^- concentration, and the difference between the presence of a regeneration mechanism and its absence becomes smaller as $[NO_3^-]_0/[formate]_0$ increases (Figure S17a, c, and e), supporting the hypothesis. Because NO is mainly produced from nitrite photolysis in the present study, continuous consumption of

https://doi.org/10.1021/acs.est.0c08199
Environ. Sci. Technol. 2021, 55, 5711−5720

NO via the NO_3^- regeneration may inhibit the recombination of photoproducts for nitrite regeneration. As a result, a slight decrease in $[NO_2^-]_P$ was observed after 780 min (Figure 4a).

ATMOSPHERIC IMPLICATION

This work provides insights into the Gly oxidation by OH radicals during particulate nitrate photolysis at aerosol-relevant concentration of Gly. Several previous studies[22−25] have indicated that glyoxal can react with OH radicals irreversibly to form organic acids (e.g., oxalic acid) in cloud/fog droplets during daylight hours. In wet aerosol, irreversible reactions of Gly with OH radicals or radical−radical reactions will produce oligomers.[20,27,28] In the present study, formic acid/formate was found as the major photooxidation product from oxidation of concentrated glyoxal. This finding suggested that oxidation of Gly at high concentration by OH radicals generated from particulate nitrate photolysis produces formate/formic acid, which may evaporate due to its high vapor pressure or is then further converted to CO_2/CO_3^{2-}. Hence, such an oxidation process may play a minor role in SOA formation in aerosol particles. Note that OH radicals in the aqueous phase can also be produced via other well-known sources, such as direct uptake from the gas phase, hydrogen peroxide photolysis, and Fenton reactions.[13,41,47] Carlton et al.[23] also reported the direct formation of formic acid via oxidation of aqueous Gly by OH radicals generated from photolysis of hydrogen peroxide, although oxalic acid was detected as another major product. Additionally, the rapidly emerging formate production through Gly oxidation by nitrite photolysis found in this study confirms the key role of OH radicals, irrespective of their source. Therefore, in principle, the present finding is not limited to particulate nitrate photolysis as the source of OH radicals. Also, the OH radical concentration ($\sim 10^{-15}$ M) estimated from our kinetic modeling falls in the reported field measurements of OH concentration with a range of $(0.1-6) \times 10^{-15}$ M in concentrated aerosols.[48] We consider that the present study with $NaNO_3$ is more pertinent in coarse-mode aerosols (e.g., aged sea-salt aerosols), whereas experiments with NH_4NO_3 would be more relevant to fine-mode aerosols. Further experiments with NH_4NO_3 are ongoing in our laboratory to investigate the product distribution when brown carbon, formed via reaction of Gly with ammonia,[49,50] is present in the particles.

Formic acid is one of the most abundant monocarboxylic acids and contributes substantially to atmospheric acidity.[51] It can catalyze the hydrolysis of sulfur trioxide (SO_3) to generate sulfuric acid (H_2SO_4) production,[52] another important contributor to acidity, and further enhance reactive uptake of oxygenated organic compounds onto acidic particles to yield SOA production.[53] Formic acid can be emitted directly from vehicle exhaust, biomass burning, terrestrial vegetation,[54,55] and secondary formation via photochemical oxidation of VOCs including glyoxal.[51] A number of studies have proposed several potential secondary atmospheric sources of formic acid: for instance, OH oxidation of α-hydroxy carbonyls[56] and isoprene nitrates,[57] oxidation of ketene-enols by O_3 and OH,[51] and reaction of Criegee intermediate CH_2OO with water vapor.[58] However, predicted formic acid concentrations based on such well-known pathways are 2−3 times lower than those of the field observations.[55] The current knowledge of formic acid production via aqueous aerosol and cloud chemistry is rather limited. For example, Xu et al.[59] found that a thermodynamic model (E-AIM IV) significantly underestimated the concentration of particulate formic acid, possibly resulting from organic salt formation as well as external mixing of formic acid with nonvolatile cations. They proposed that missing photochemical processes may play a potential role in formic acid production since their observation results showed evident midday peaks of gaseous and particulate formic acid concentration in the summer.[59] The oxidation of Gly promoted by particulate nitrate photolysis provides a novel pathway for in-particle formic acid/formate production, which may partially narrow the gap between the model prediction and the field measurements.

In addition to formic acid production, oxidation of Gly during particulate nitrate photolysis may partially contribute to the sink of Gly in the atmosphere. Typically, the main loss pathways of Gly include gas-phase photolysis, reaction with OH, dry deposition, and partitioning into aerosols, among which Gly uptake by aerosols is the most complicated and needs more comprehensive exploration.[19] However, recent work has suggested that the model overpredicted the mixing ratios of glyoxal by a factor of 3.3 compared to the observed levels without considering the heterogeneous processes of Gly on aerosol surfaces in the Pearl River Delta (PRD) region.[19] Previous studies also reported that the simulations with only the gas-phase schemes overpredicted the Gly concentration by factors of 2−6 in both urban Mexico City[60] and a semirural site of the PRD region.[61] The significant overestimation suggested that there were missing loss pathways for Gly, such as heterogeneous reaction processes. Efficient oxidation of Gly promoted by particulate nitrate photolysis demonstrated in this study may potentially contribute to the sink of Gly in the atmosphere.

ASSOCIATED CONTENT

Supporting Information

The Supporting Information is available free of charge at https://pubs.acs.org/doi/10.1021/acs.est.0c08199.

Texts describing estimation of irradiation intensity and calculation of the photolysis rate constant (j_{NO3-}, j_{NO2-}, and j_{H2O2}), Gly structures in particles, and the reaction of CO_3^{2-} with Gly; tables listing reactions of Gly oxidation during nitrate photolysis and initial concentration of nitrate and Gly at different $[NO_3^-]_0/[Gly]_0$; figures showing particle size and normalized Raman peak area ratios as a function of equilibrium time, in situ Raman spectroscopy/flow cell setup, Raman and IC analysis of irradiated $NaNO_3$ + Gly, particle pH as reaction proceeds, calibration curve of sodium formate and sodium nitrate, $[NO_3^-]_P$, $[Gly]_P$, $[NO_3^-]_M$, and $A(Gly)/A(OH)_{water}$ at different $[NO_3^-]_0/[Gly]_0$, Raman spectra of $NaNO_3$ + Gly + dark in air and Na_2SO_4 + Gly + UV in air, formate production under different light intensities, normalized formate production as a function of time, kinetic model results of relationship between d[formate]/d t and $[NO_3^-]_0$, change of particle size during reaction, sensitivity test of the $[H_2O_2$ pathway$]_f$, Gly oxidation by nitrite photolysis, Raman spectra of irradiated $NaNO_3$ + Gly under 254 nm irradiation, $[formate]_P$ in the absence of the $[OH$ pathway$]_f$ or $[H_2O_2$ pathway$]_f$, $[formate]_M$ as a function of time of premixed $NaNO_3$ + formate under dark conditions or UV irradiation, $[formate]_P$ and $[NO_3^-]_P$ at different $[NO_3^-]_0/[formate]_0$ under 300 nm irradiation, time

https://doi.org/10.1021/acs.est.0c08199
Environ. Sci. Technol. 2021, 55, 5711−5720

evolution of $[NO_3^-]_M$ at different $[NO_3^-]_0/[formate]_0$ in air and N_2, reproduced formate concentration and predicted oxidant concentration at different $[NO_3^-]_0/[Gly]_0$, photodecay plot and molar absorptivity of 2NB, Raman spectrum of pure particulate Gly at 80% RH, Raman spectra of NO_3^- and CO_3^{2-} at $[NO_3^-]_0/[Gly]_0 = 1$, and time evolution of the normalized peak area of CO_3^{2-} and Gly of premixed Na_2CO_3 + Gly (PDF)

AUTHOR INFORMATION

Corresponding Authors

Masao Gen − *Faculty of Frontier Engineering, Institute of Science and Engineering, Kanazawa University, Kanazawa 920-1192, Japan;* orcid.org/0000-0001-6160-9029; Email: mgen@staff.kanazawa-u.ac.jp

Chak K. Chan − *School of Energy and Environment, City University of Hong Kong, Kowloon, Hong Kong, China;* orcid.org/0000-0001-9687-8771; Phone: +(852)-3442-5593; Email: chak.k.chan@cityu.edu.hk; Fax: +(852)-3442-068

Authors

Ruifeng Zhang − *School of Energy and Environment, City University of Hong Kong, Kowloon, Hong Kong, China;* orcid.org/0000-0003-2361-1990

Tzung-May Fu − *School of Environmental Science and Engineering, Southern University of Science and Technology, Shenzhen 518055, China;* orcid.org/0000-0002-8556-7326

Complete contact information is available at: https://pubs.acs.org/10.1021/acs.est.0c08199

Notes

The authors declare no competing financial interest.

ACKNOWLEDGMENTS

We gratefully acknowledge support from the National Natural Science Foundation of China (42075100 and 41875142) and the Guangdong Basic and Applied Basic Research Foundation (2020B1515130003). This work was also supported in part by the Japan Society for the Promotion of Science KAKENHI Grant-in-Aid for Research Activity Start-up (20K23363), the Kurita Water and Environment Foundation (20A030), the Steel Foundation for Environmental Protection Technology, and The Sumitomo Foundation (203113).

REFERENCES

(1) Chan, C. K.; Yao, X. Air pollution in mega cities in China. *Atmos. Environ.* **2008**, *42*, 1−42.

(2) Yao, X.; Chan, C. K.; Fang, M.; Cadle, S.; Chan, T.; Mulawa, P.; He, K.; Ye, B. The water-soluble ionic composition of $PM_{2.5}$ in Shanghai and Beijing, China. *Atmos. Environ.* **2002**, *36*, 4223−4234.

(3) Benedict, K. B.; McFall, A. S.; Anastasio, C. Quantum yield of nitrite from the photolysis of aqueous nitrate above 300 nm. *Environ. Sci. Technol.* **2017**, *51*, 4387−4395.

(4) Ye, C.; Zhang, N.; Gao, H.; Zhou, X. Photolysis of Particulate Nitrate as a Source of HONO and NO_x. *Environ. Sci. Technol.* **2017**, *51*, 6849−6856.

(5) Romer, P. S.; Wooldridge, P. J.; Crounse, J. D.; Kim, M. J.; Wennberg, P. O.; Dibb, J. E.; Scheuer, E.; Blake, D. R.; Meinardi, S.; Brosius, A. L.; Thames, A. B.; Miller, D. O.; Brune, W. H.; Hall, S. R.; Ryerson, T. B.; Cohen, R. C. Constraints on Aerosol Nitrate Photolysis as a Potential Source of HONO and NO_x. *Environ. Sci. Technol.* **2018**, *52*, 13738−13746.

(6) Gen, M.; Zhang, R.; Huang, D. D.; Li, Y.; Chan, C. K. Heterogeneous SO_2 Oxidation in Sulfate Formation by Photolysis of Particulate Nitrate. *Environ. Sci. Technol. Lett.* **2019**, *6*, 86−91.

(7) Gen, M.; Zhang, R.; Huang, D. D.; Li, Y.; Chan, C. K. Heterogeneous Oxidation of SO_2 in Sulfate Production during Nitrate Photolysis at 300 nm: Effect of pH, Relative Humidity, Irradiation Intensity, and the Presence of Organic Compounds. *Environ. Sci. Technol.* **2019**, *53*, 8757−8766.

(8) Zhang, R.; Gen, M.; Huang, D.; Li, Y.; Chan, C. K. Enhanced Sulfate Production by Nitrate Photolysis in the Presence of Halide Ions in Atmospheric Particles. *Environ. Sci. Technol.* **2020**, *54*, 3831−3839.

(9) Bao, F.; Jiang, H.; Zhang, Y.; Li, M.; Ye, C.; Wang, W.; Ge, M.; Chen, C.; Zhao, J. The Key Role of Sulfate in the Photochemical Renoxification on Real $PM_{2.5}$. *Environ. Sci. Technol.* **2020**, *54*, 3121−3128.

(10) Zheng, H.; Song, S.; Sarwar, G.; Gen, M.; Wang, S.; Ding, D.; Chang, X.; Zhang, S.; Xing, J.; Sun, Y.; Ji, D.; Chan, C. K.; Gao, J.; McElroy, M. B. Contribution of Particulate Nitrate Photolysis to Heterogeneous Sulfate Formation for Winter Haze in China. *Environ. Sci. Technol. Lett.* **2020**, *7*, 632−638.

(11) Akherati, A.; He, Y.; Coggon, M. M.; Koss, A. R.; Hodshire, A. L.; Sekimoto, K.; Warneke, C.; de Gouw, J.; Yee, L.; Seinfeld, J. H.; Onasch, T. B.; Herndon, S. C.; Knighton, W. B.; Cappa, C. D.; Kleeman, M. J.; Lim, C. Y.; Kroll, J. H.; Pierce, J. R.; Jathar, S. H. Oxygenated aromatic compounds are important precursors of secondary organic aerosol in biomass-burning emissions. *Environ. Sci. Technol.* **2020**, *54*, 8568−8579.

(12) Hallquist, M.; Wenger, J. C.; Baltensperger, U.; Rudich, Y.; Simpson, D.; Claeys, M.; Dommen, J.; Donahue, N.; George, C.; Goldstein, A.; Hamilton, J. F.; Herrmann, H.; Hoffmann, T.; Iinuma, Y.; Jang, M.; Jenkin, M. E.; Jimenez, J. L.; Kiendler-Scharr, A.; Maenhaut, W.; McFiggans, G.; Mentel, T. F.; Monod, A.; Prévôt, A. S. H.; Seinfeld, J. H.; Surratt, J. D.; Szmigielski, R.; Wildt, J. The formation, properties and impact of secondary organic aerosol: current and emerging issues. *Atmos. Chem. Phys.* **2009**, *9*, 5155−5236.

(13) Ervens, B.; Sorooshian, A.; Lim, Y. B.; Turpin, B. J. Key parameters controlling OH-initiated formation of secondary organic aerosol in the aqueous phase (aqSOA). *J. Geophys. Res. Atmos.* **2014**, *119*, 3997−4016.

(14) Volkamer, R.; Jimenez, J. L.; San Martini, F.; Dzepina, K.; Zhang, Q.; Salcedo, D.; Molina, L. T.; Worsnop, D. R.; Molina, M. J. Secondary organic aerosol formation from anthropogenic air pollution: Rapid and higher than expected. *Geophys. Res. Lett.* **2006**, *33*, L17811.

(15) Heald, C. L.; Jacob, D. J.; Park, R. J.; Russell, L. M.; Huebert, B. J.; Seinfeld, J. H.; Liao, H.; Weber, R. J. A large organic aerosol source in the free troposphere missing from current models. *Geophys. Res. Lett.* **2005**, *32*, L18809.

(16) Monge, M. E.; Rosenørn, T.; Favez, O.; Müller, M.; Adler, G.; Riziq, A. A.; Rudich, Y.; Herrmann, H.; George, C.; D'Anna, B. Alternative pathway for atmospheric particles growth. *Proc. Natl. Acad. Sci. U. S. A.* **2012**, *109*, 6840−6844.

(17) Huang, D. D.; Zhang, Q.; Cheung, H. H. Y.; Yu, L.; Zhou, S.; Anastasio, C.; Smith, J. D.; Chan, C. K. Formation and evolution of aqSOA from aqueous-phase reactions of phenolic carbonyls: comparison between ammonium sulfate and ammonium nitrate solutions. *Environ. Sci. Technol.* **2018**, *52*, 9215−9224.

(18) Schaefer, T.; Van Pinxteren, D.; Herrmann, H. Multiphase chemistry of glyoxal: Revised kinetics of the alkyl radical reaction with molecular oxygen and the reaction of glyoxal with OH, NO_3, and SO_4^- in aqueous solution. *Environ. Sci. Technol.* **2015**, *49*, 343−350.

(19) Ling, Z.; Xie, Q.; Shao, M.; Wang, Z.; Wang, T.; Guo, H.; Wang, X. Formation and sink of glyoxal and methylglyoxal in a polluted subtropical environment: observation-based photochemical analysis and impact evaluation. *Atmos. Chem. Phys.* **2020**, *20*, 11451−11467.

(20) Lim, Y. B.; Tan, Y.; Perri, M. J.; Seitzinger, S. P.; Turpin, B. J. Aqueous chemistry and its role in secondary organic aerosol (SOA) formation. *Atmos. Chem. Phys.* **2010**, *10*, 10521−10539.
(21) McNeill, V. F. Aqueous Organic Chemistry in the Atmosphere: Sources and Chemical Processing of Organic Aerosols. *Environ. Sci. Technol.* **2015**, *49*, 1237−1244.
(22) Tan, Y.; Perri, M. J.; Seitzinger, S. P.; Turpin, B. J. Effects of precursor concentration and acidic sulfate in aqueous glyoxal-OH radical oxidation and implications for secondary organic aerosol. *Environ. Sci. Technol.* **2009**, *43*, 8105−8112.
(23) Carlton, A. G.; Turpin, B. J.; Altieri, K. E.; Seitzinger, S.; Reff, A.; Lim, H.-J.; Ervens, B. Atmospheric oxalic acid and SOA production from glyoxal: Results of aqueous photooxidation experiments. *Atmos. Environ.* **2007**, *41*, 7588−7602.
(24) Zhang, F.; Yu, X.; Sui, X.; Chen, J.; Zhu, Z.; Yu, X.-Y. Evolution of aqSOA from the Air-Liquid Interfacial Photochemistry of Glyoxal and Hydroxyl Radicals. *Environ. Sci. Technol.* **2019**, *53*, 10236−10245.
(25) Lee, A. K. Y.; Zhao, R.; Gao, S. S.; Abbatt, J. P. D. Aqueous-phase OH oxidation of glyoxal: application of a novel analytical approach employing aerosol mass spectrometry and complementary off-line techniques. *J. Phys. Chem. A* **2011**, *115*, 10517−10526.
(26) Volkamer, R.; Ziemann, P. J.; Molina, M. J. Secondary Organic Aerosol Formation from Acetylene (C_2H_2): seed effect on SOA yields due to organic photochemistry in the aerosol aqueous phase. *Atmos. Chem. Phys.* **2009**, *9*, 1907−1928.
(27) De Haan, D. O.; Corrigan, A. L.; Tolbert, M. A.; Jimenez, J. L.; Wood, S. E.; Turley, J. J. Secondary organic aerosol formation by self-reactions of methylglyoxal and glyoxal in evaporating droplets. *Environ. Sci. Technol.* **2009**, *43*, 8184−8190.
(28) Loeffler, K. W.; Koehler, C. A.; Paul, N. M.; De Haan, D. O. Oligomer formation in evaporating aqueous glyoxal and methyl glyoxal solutions. *Environ. Sci. Technol.* **2006**, *40*, 6318−6323.
(29) Mack, J.; Bolton, J. R. Photochemistry of nitrite and nitrate in aqueous solution: a review. *J. Photochem. Photobiol., A* **1999**, *128*, 1−13.
(30) Zheng, B.; Zhang, Q.; Zhang, Y.; He, K. B.; Wang, K.; Zheng, G. J.; Duan, F. K.; Ma, Y. L.; Kimoto, T. Heterogeneous chemistry: a mechanism missing in current models to explain secondary inorganic aerosol formation during the January 2013 haze episode in North China. *Atmos. Chem. Phys.* **2015**, *15*, 2031−2049.
(31) Galbavy, E. S.; Ram, K.; Anastasio, C. 2-Nitrobenzaldehyde as a chemical actinometer for solution and ice photochemistry. *J. Photochem. Photobiol., A* **2010**, *209*, 186−192.
(32) Chen, G.; Hanukovich, S.; Chebeir, M.; Christopher, P.; Liu, H. Nitrate Removal via a Formate Radical-Induced Photochemical Process. *Environ. Sci. Technol.* **2019**, *53*, 316−324.
(33) Socrates, G. *Infrared and Raman characteristic group frequencies: tables and charts*; Wiley: New York, 2004.
(34) Malik, M.; Joens, J. A. Temperature dependent near-UV molar absorptivities of glyoxal and gluteraldehyde in aqueous solution. *Spectrochim. Acta A Mol. Biomol. Spectrosc.* **2000**, *56*, 2653−2658.
(35) Parandaman, A.; Kumar, M.; Francisco, J. S.; Sinha, A. Organic acid formation from the atmospheric oxidation of gem diols: reaction mechanism, energetics, and rates. *J. Phys. Chem. A* **2018**, *122*, 6266−6276.
(36) Haag, W. R.; Yao, C. C. D. Rate constants for reaction of hydroxyl radicals with several drinking water contaminants. *Environ. Sci. Technol.* **1992**, *26*, 1005−1013.
(37) Zhao, R.; Lee, A. K. Y.; Abbatt, J. P. D. Investigation of aqueous-phase photooxidation of glyoxal and methylglyoxal by aerosol chemical ionization mass spectrometry: observation of hydroxyhydroperoxide formation. *J. Phys. Chem. A* **2012**, *116*, 6253−6263.
(38) Nozière, B.; Dziedzic, P.; Córdova, A. Inorganic ammonium salts and carbonate salts are efficient catalysts for aldol condensation in atmospheric aerosols. *Phys. Chem. Chem. Phys.* **2010**, *12*, 3864−3872.
(39) Avzianova, E.; Brooks, S. D. Raman spectroscopy of glyoxal oligomers in aqueous solutions. *Spectrochim. Acta A Mol. Biomol. Spectrosc.* **2013**, *101*, 40−48.
(40) Wilson, K. R.; Prophet, A. M.; Rovelli, G.; Willis, M. D.; Rapf, R. J.; Jacobs, M. I. A kinetic description of how interfaces accelerate reactions in micro-compartments. *Chem. Sci.* **2020**, *11*, 8533−8545.
(41) Gligorovski, S.; Strekowski, R.; Barbati, S.; Vione, D. Environmental implications of hydroxyl radicals (•OH). *Chem. Rev.* **2015**, *115*, 13051−13092.
(42) Saghafi, H.; Vahedpour, M.; Douroudgari, H. Complete degradation of Glyoxal by NO radicals through two steps: The first at high-temperatures and the second at low-temperatures. *Comput. Theor. Chem.* **2020**, *1180*, 112822.
(43) Thomas, J. Gas-phase reactions of nitrogen dioxide. Part 2. The oxidation of glyoxal. *Trans. Faraday Soc.* **1953**, *49*, 630−635.
(44) Saghafi, H.; Vahedpour, M. Atmospheric reactions of glyoxal with NO_2 and NH_2 radicals: Hydrogen abstraction mechanism and natural bond orbital analysis. *Prog. React. Kinet. Mech.* **2019**, *44*, 187−209.
(45) Girod, M.; Moyano, E.; Campbell, D. I.; Cooks, R. G. Accelerated bimolecular reactions in microdroplets studied by desorption electrospray ionization mass spectrometry. *Chem. Sci.* **2011**, *2*, 501−510.
(46) Goldstein, S.; Rabani, J. Mechanism of nitrite formation by nitrate photolysis in aqueous solutions: the role of peroxynitrite, nitrogen dioxide, and hydroxyl radical. *J. Am. Chem. Soc.* **2007**, *129*, 10597−10601.
(47) Deguillaume, L.; Leriche, M.; Chaumerliac, N. Impact of radical versus non-radical pathway in the Fenton chemistry on the iron redox cycle in clouds. *Chemosphere* **2005**, *60*, 718−724.
(48) Tilgner, A.; Herrmann, H. Tropospheric Aqueous-Phase OH Oxidation Chemistry: Current Understanding, Uptake of Highly Oxidized Organics and Its Effects. *Multiphase Environ. Chem. Atmos.* **2018**, *1299*, 49−85.
(49) Yu, G.; Bayer, A. R.; Galloway, M. M.; Korshavn, K. J.; Fry, C. G.; Keutsch, F. N. Glyoxal in aqueous ammonium sulfate solutions: products, kinetics and hydration effects. *Environ. Sci. Technol.* **2011**, *45*, 6336−6342.
(50) Gen, M.; Huang, D. D.; Chan, C. K. Reactive uptake of glyoxal by ammonium-containing salt particles as a function of relative humidity. *Environ. Sci. Technol.* **2018**, *52*, 6903−6911.
(51) Wang, S.; Newland, M. J.; Deng, W.; Rickard, A. R.; Hamilton, J. F.; Muñoz, A.; Ródenas, M.; Vázquez, M. M.; Wang, L.; Wang, X. Aromatic Photooxidation, A New Source of Atmospheric Acidity. *Environ. Sci. Technol.* **2020**, *54*, 7798−7806.
(52) Hazra, M. K.; Sinha, A. Formic acid catalyzed hydrolysis of SO_3 in the gas phase: A barrierless mechanism for sulfuric acid production of potential atmospheric importance. *J. Am. Chem. Soc.* **2011**, *133*, 17444−17453.
(53) Jang, M.; Czoschke, N. M.; Lee, S.; Kamens, R. M. Heterogeneous atmospheric aerosol production by acid-catalyzed particle-phase reactions. *Science* **2002**, *298*, 814−817.
(54) Chaliyakunnel, S.; Millet, D. B.; Wells, K. C.; Cady-Pereira, K. E.; Shephard, M. W. A large underestimate of formic acid from tropical fires: constraints from space-borne measurements. *Environ. Sci. Technol.* **2016**, *50*, 5631−5640.
(55) Millet, D. B.; Baasandorj, M.; Farmer, D. K.; Thornton, J. A.; Baumann, K.; Brophy, P.; Chaliyakunnel, S.; de Gouw, J. A.; Graus, M.; Hu, L.; Koss, A.; Lee, B. H.; Lopez-Hilfiker, F. D.; Neuman, J. A.; Paulot, F.; Peischl, J.; Pollack, I. B.; Ryerson, T. B.; Warneke, C.; Williams, B. J.; Xu, J. A large and ubiquitous source of atmospheric formic acid. *Atmos. Chem. Phys.* **2015**, *15*, 6283−6304.
(56) Butkovskaya, N. I.; Pouvesle, N.; Kukui, A.; Le Bras, G. Mechanism of the OH-initiated oxidation of glycolaldehyde over the temperature range 233-296 K. *J. Phys. Chem. A* **2006**, *110*, 13492−13499.
(57) Paulot, F.; Crounse, J. D.; Kjaergaard, H. G.; Kroll, J. H.; Seinfeld, J. H.; Wennberg, P. O. Isoprene photooxidation: new

https://doi.org/10.1021/acs.est.0c08199
Environ. Sci. Technol. 2021, 55, 5711−5720

insights into the production of acids and organic nitrates. *Atmos. Chem. Phys.* **2009**, *9*, 1479−1501.
(58) Francisco, J. S.; Eisfeld, W. Atmospheric oxidation mechanism of hydroxymethyl hydroperoxide. *J. Phys. Chem. A* **2009**, *113*, 7593−7600.
(59) Xu, J.; Chen, J.; Shi, Y.; Zhao, N.; Qin, X.; Yu, G.; Liu, J.; Lin, Y.; Fu, Q.; Weber, R. J.; Lee, S.-H.; Deng, C.; Huang, K. First Continuous Measurement of Gaseous and Particulate Formic Acid in a Suburban Area of East China: Seasonality and Gas-Particle Partitioning. *ACS Earth Space Chem.* **2019**, *4*, 157−167.
(60) Volkamer, R.; San Martini, F.; Molina, L. T.; Salcedo, D.; Jimenez, J. L.; Molina, M. J. A missing sink for gas-phase glyoxal in Mexico City: Formation of secondary organic aerosol. *Geophys. Res. Lett.* **2007**, *34*, L19807.
(61) Li, X.; Rohrer, F.; Brauers, T.; Hofzumahaus, A.; Lu, K.; Shao, M.; Zhang, Y. H.; Wahner, A. Modeling of HCHO and CHOCHO at a semi-rural site in southern China during the PRIDE-PRD2006 campaign. *Atmos. Chem. Phys.* **2014**, *14*, 12291−12305.

https://doi.org/10.1021/acs.est.0c08199
Environ. Sci. Technol. 2021, 55, 5711−5720